



Article

# A Simplified Model to Predict the Repeated Shear Strain during the Cyclic Triaxial Test by Using an Elastic Coefficient-Damping Ratio System

Darn-Horng Hsiao \*D, Yao-Wen Liang and Chia-Sheng Hsieh D

 $Department \ of \ Civil \ Engineering, \ National \ Kaohsiung \ University \ of \ Science \ and \ Technology, 415 \ Chien \ Kung \ Road, \ Kaohsiung \ 80778, \ Taiwan; \ f111141104@nkust.edu.tw \ (Y.-W.L.); \ hsieh@nkust.edu.tw \ (C.-S.H.)$ 

\* Correspondence: hsiaodh@nkust.edu.tw; Tel.: +886-73-814-526 (ext. 15259)

Abstract: Some researchers in past years have tried to develop a simplified method for analyzing soil liquefaction. However, the correctness of the pore water pressure in the model will affect the results. In addition, the formulas derived are not easy, and the exact parameters of the model are difficult to obtain. This study used a mass-spring-damping system to simulate the repeated strain of liquefaction cyclic triaxial tests. Because the model is simple and the parameters are easy to understand and obtain, it also shows the extensibility of this model. During the parameter study, damping coefficient c and spring coefficient k parameters decreased with the increasing cyclic number. Preliminary results of the research show that this model can further simulate the repeated strain obtained by cyclic triaxial tests without considering the variation of effective stress during cyclic loading. Four samples were used to verify the model's correctness, and their boring sites were found in Yunlin areas, Taiwan. Simulation results show that the spring-damping system is feasible for simulated cyclic triaxial tests because the simulated results correlate to the testing results in trend. Generally, the first cycle number simulation will be less accurate because the pore water pressure of the specimen changes rapidly when the performance has just started. In contrast, the increase in subsequent cycles may be biased due to cyclic stress variation and soil plasticity during simulation. In the future, pure sand specimens created in the laboratory will be suggested for simulation.

**Keywords:** spring-damping system; liquefaction during cyclic triaxial test; repeated strain; spring coefficient; damping coefficient



Citation: Hsiao, D.-H.; Liang, Y.-W.; Hsieh, C.-S. A Simplified Model to Predict the Repeated Shear Strain during the Cyclic Triaxial Test by Using an Elastic Coefficient-Damping Ratio System. *Appl. Sci.* **2024**, *14*, 4178. https://doi.org/10.3390/app14104178

Academic Editor: Tiago Miranda

Received: 4 April 2024 Revised: 12 May 2024 Accepted: 13 May 2024 Published: 15 May 2024



Copyright: © 2024 by the authors. Licensee MDPI, Basel, Switzerland. This article is an open access article distributed under the terms and conditions of the Creative Commons Attribution (CC BY) license (https://creativecommons.org/licenses/by/4.0/).

# 1. Introduction

In past years, many mathematical models have been developed for analyzing ground seismic liquefaction. For the simulation target for the cyclic triaxial test, previous examples considered pore water pressure. Research [1,2] mentioned that simplified mathematical models can predict soil liquefaction phenomena under dynamic load. However, the correctness of the pore water pressure in the model will affect the results. Three different models accompanied by parameters were used to simulate pore water pressure [3–5]. The most significant difficulty in this related research is that the formulas developed are difficult to derive, and the parameters of the mathematical model are not easy to obtain [6–12].

The mass-spring-damping system has been used [6,7] to design the foundation of the hammer and press base and the structural analysis between the piers and supports, both of which were based on the mass-spring-damping system. Design and analysis were commonly seen in structural dynamics-related research but less conducted in geotechnical engineering.

The soil shear modulus (G) and damping ratio (D) can be determined with cyclic triaxial tests [13–15]. However, Varghese et al. [16] found that the damping ratio D and shear modulus G of the first five cycles will decrease as the cyclic number increases. These two parameters also relate to the damping coefficient (c) and spring coefficient (k) in the mass-spring-damping system. Its trend can be used for more in-depth research and

discussion. The parameters are easy to understand and obtain, showing the extensibility of this model, so the mass-spring-damper system could be chosen to simulate the strain of cyclic triaxial tests. It was also found that the damping ratio may increase with shear strain but reverse under large shear strains [17]. The damping ratio will decrease when the specimen increases with the dynamic strain [18].

As for the waste soil materials, the damping ratio first decreased and then increased as the shear strain increased using a cyclic triaxial instrument [19]. Some researchers [20–24] also used a viscoelastic–plastic model for soil stiffness degradation and damping ratio and applied it to related engineering. As for regional studies, Chattaraj and Sengupta [25] discussed Kasai River sand in India using a model. Xu et al. [26] analyzed and compared the model and test results of undrained repeated triaxial tests on densely saturated sand with different particle sizes and fine content. They also used the equivalent granular state parameter to discuss the model parameters.

The repeated strain of soil is generally obtained through laboratory liquefaction cyclic triaxial tests, and relevant research is conducted under the conditions of many influencing factors such as material type, particle size, gradation, etc. This paper attempts to develop a mathematical model using the mass-spring-damper system, discusses whether both the spring coefficient and damping coefficient are variables, and studies the values of various parameters of the system, including mass m, spring coefficient k, damping coefficient c, and external force  $Q_0$ , calculated using Mathematica software. Finally, the original thintube specimens from four locations in the Yunlin area of Taiwan were selected to conduct liquefaction cyclic triaxial tests. Then, the test results were compared with the model to investigate pattern correctness.

#### 2. Methods

## 2.1. Developed Model

This study used a mass-spring-damping system to simulate the repeated strain of cyclic triaxial tests during liquefaction and investigate the related parameters of the model. Kramer (1996) [7] indicated that the formula for the mass-spring-damping system is Equation (1).

$$m\ddot{z} + c\dot{z} + kz = Q_0 \sin \Omega t \tag{1}$$

In the formula, m is the mass, c is the damping coefficient, k is the spring coefficient,  $Q_0$  is the external force, z is the displacement,  $\Omega$  is the frequency of the external force, and t is the corresponding time.

If all parameters are constants, the solution of the equation is shown in two terms. The first two terms in the equation are transitional solutions, which will tend to 0 when t >> 0, and the third is the transient solution. The formulas of the transition and transient solutions can also be found in Kramer's book [13]. The total solution is shown in Equation (2), which is the sum of the transition and steady-state solutions. The transition solution can be obtained by Equation (3), which is an unstable solution that changes irregularly with time. The steady-state solution can be obtained by Equation (4), a stable solution that trends as a sinusoidal function over time.

$$u_t(t) = u_c(t) + u_p(t) \tag{2}$$

$$u_c(t) = \frac{Q_0}{k} \frac{1}{\left(1 - \beta^2\right)^2 + \left(2\xi\beta\right)^2} e^{-\xi\omega_0 t} \left[ \frac{\overline{\omega}}{\omega_d} \left(\beta^2 + 2\xi^2 - 1\right) \sin\omega_d t + 2\xi\beta\cos\omega_d t \right] \quad (3)$$

$$u_{p}(t) = \frac{Q_{0}}{k} \frac{1}{\left(1 - \beta^{2}\right)^{2} + \left(2\xi\beta\right)^{2}} \left[\left(1 - \beta^{2}\right)\sin\overline{\omega}t - 2\xi\beta\cos\overline{\omega}t\right] \tag{4}$$

where natural frequency  $\omega_0=\sqrt{\frac{k}{m}}$ , damping ratio  $\xi=\frac{c}{2m\omega_0}$ , damping ratio natural frequency  $\omega_d=\omega_0\sqrt{1-\xi^2}$ ,  $\beta=\frac{\overline{\omega}}{\omega_0}$ .

Appl. Sci. 2024, 14, 4178 3 of 20

## 2.2. Parameter Study

To verify the correctness of the model, the samples were selected, and boring sites were found in the Tuku and Huwei areas in Yunlin, Taiwan. In 1999, the 921 Chi-Chi earthquake impacted the central regions of Taiwan. The earthquake's epicenter was about 20 km away from this sampling site base. Dozens of people were killed in the Yunlin area at that time. Hwang et al. and Chang et al. [27,28] conducted a liquefaction analysis in the Yunlin area of the 921 Chi-Chi earthquake. In recent years, Fansuri et al. and Chiou et al. [29,30] also conducted follow-up related research on the Yunlin area. Figure 1 shows the sampling base site and the location of the Yunlin area in Taiwan. This study selected four locations for drilling and sampling. Subsequently, the original thin-tube specimen at site A will be used as the result of the reference example. In this study, undisturbed thin-tube specimens from four locations in Yunlin, Taiwan, were selected to simulate the strain of the specimen through a mass-spring-damping system, namely sites A, B, C, and D. Their locations are shown in Figure 1; the test specimens were selected based on the liquefaction potential value (LPI, liquefaction potential index can be judged liquefaction potential for local area) obtained through the relevant physical properties and SPT N value test results (standard penetration test N related with soil strength). This study selected two test specimens in the medium liquefaction potential area and two in the high liquefaction potential area. Table 1 shows cyclic triaxial test results of twelve specimens taken from four sites. Four specimens will be further analyzed for the strain value by the mass-spring-damping system to compare those of cyclic triaxial test specimens. Das [31] explained boring and sampling very clearly. Kaya and Erken and Bray et al. [32,33] also used the thin-tube method to obtain the samples to be tested afterward. We also referred to their suggestion and requirements during the boring and sampling period.

**Table 1.** Cyclic triaxial test results of 12 specimens obtained from four sites.

Specimen No.	B (%)	Soil Density (t/m³)	Water Content (%)	Soil Type (USCS *)	$G_s$	Confined Pressure σ' <sub>c</sub> (kPa)	Cyclic Stress σ <sub>dp</sub> (kPa)	CSR	Liquefied Cyclic No.	CRR <sub>7.5</sub>
A-1	>95	2.02	16.09	SP-SM	2.76	100	54.51	0.273	12	0.253
A-2	>95	2.02	16.09	SP-SM	2.76	100	49.49	0.247	15	0.253
A-3	>95	2.02	16.09	SP-SM	2.76	100	42.24	0.211	24	0.253
B-1	>95	2.02	22.44	SW-SM	2.69	90	57.10	0.317	8	0.266
B-2	>95	2.02	22.44	SW-SM	2.69	90	50.65	0.281	18	0.266
B-3	>95	2.02	22.44	SW-SM	2.69	90	39.07	0.217	20	0.266
C-1	>95	2.12	23.33	SM	2.69	100	53.02	0.265	9	0.256
C-2	>95	2.12	23.33	SM	2.69	100	50.01	0.251	20	0.256
C-3	>95	2.12	23.33	SM	2.69	100	41.94	0.209	70	0.256
D-1	>95	1.90	37.61	ML	2.57	150	58.25	0.194	13	0.172
D-2	>95	1.90	37.61	ML	2.57	150	44.09	0.147	36	0.172
D-3	>95	1.90	37.61	ML	2.57	150	59.16	0.197	3	0.172

<sup>\*</sup> Soils were classified by USCS (United Soil Classification System).

Appl. Sci. 2024, 14, 4178 4 of 20

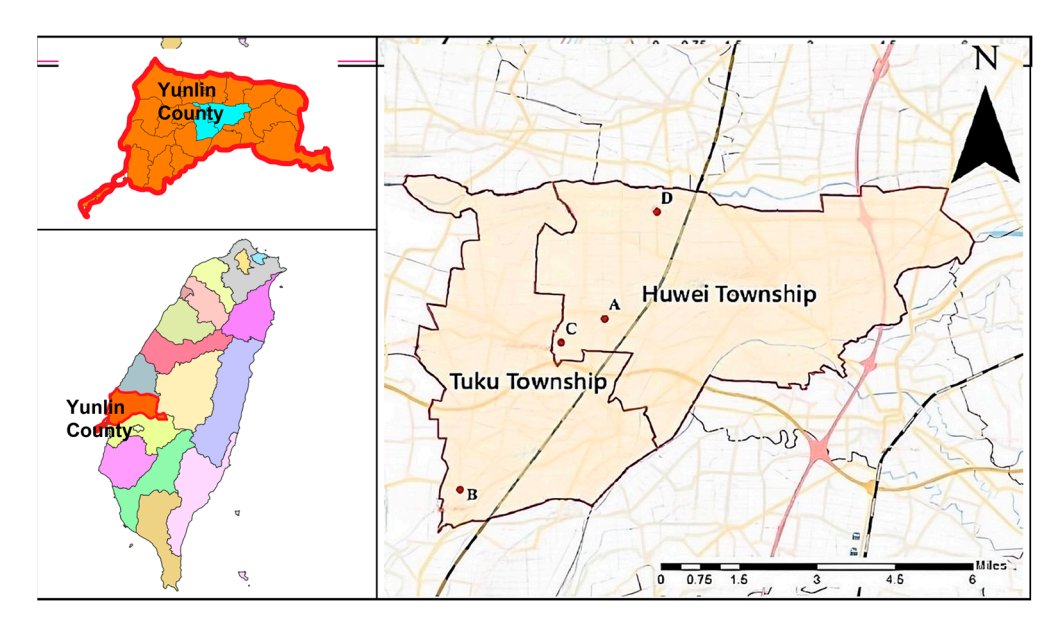


Figure 1. Undisturbed thin-tube specimens from four sites in Yunlin, Taiwan.

#### 2.2.1. Parameters Are Constant

When all coefficients are constants, the solution of the problem is as Equation (2). The first two terms in Equation (3) are transitional solutions and will tend to 0 when t >> 0; the first two terms can be regarded as 0, so only the third term in Equation (4) can be calculated to obtain the displacement. Meantime, Equation (4) can be found that the spring coefficient (k) and the damping coefficient (c) are located in the denominator and are inversely proportional to the displacement. It means that if the maximum value of the constant is substituted, then the displacement obtained will be the minimum. However, it can be known from the concepts of rising pore water pressure and falling effective stress that both variables of the spring coefficient k and the damping coefficient c will change with time. Once the spring and damping coefficients are substituted as variables, it cannot be directly solved through Equation (2). However, it can be inferred from the above. When the spring coefficient (k) and damping coefficient (c) decrease as time increases, the displacement will increase accordingly. Because the analytical solution cannot be obtained directly, we will use Mathematica software to find the numerical solution for the differential equation.

#### 2.2.2. Parameters k and c Are Variables Depending on Time

The parameters required for the mass-spring-damping system to simulate the strain of cyclic liquefaction triaxial tests are mass, spring coefficient, damping coefficient, and external force, which can be determined by the increase in pore water pressure and the decrease in effective stress. The concept can be used to obtain parameters corresponding to different specimens; when the pore water pressure of the specimen in cyclic triaxial tests increases, it will cause the specimen to liquefy, causing the effective stress, shear modulus G, and damping ratio D to decrease, causing the strain to increase, and the shear modulus G and damping ratio D are related to the spring coefficient k and damping coefficient c, respectively. Both are variables that change with time. This study uses the original thin-tube specimen at site A in the Yunlin area as an example for parameter calculation. Akbarimehr and Fakharian [19] mentioned the relationship between stiffness degradation, damping, and shear strain. Pisanò and Jeremić [20] also mentioned the relationship between stiffness degradation and damping.

#### Mass

The mass of point A is calculated as follows. The mass (m) is calculated by multiplying the volume of the specimen in the cyclic triaxial test by the unit weight of the soil. It is known that the diameter and height of the specimen are 7.1 cm and 14.2 cm, respectively.

Appl. Sci. 2024, 14, 4178 5 of 20

Thus, the calculated volume is  $562.2 \text{ cm}^2$ . The unit weight of the cyclic triaxial test specimen could change with the soil gradation or soil types, generally in the range between  $1.9 \text{ and } 2.12 \text{ g/cm}^3$  in Table 1. After multiplying the volume of the specimen by the unit weight, the available mass heavier than most soils generally falls between 800 and 1000 g, so each specimen's mass m is defined to be 1 kg in the study.

## Spring Coefficient

The spring coefficient (k) of the reference sample A is calculated by dividing the force F by the length change  $\Delta L$ , as shown in Equation (5), where the force and the length change are computed at a strain of 1%. When calculating the external force, the axial differential stress  $(\sigma_1 - \sigma_3)$  in the formula is obtained from the static triaxial undrained CU test results of Hsiao et al. [34]. It is found that the axial differential stress 78 kPa can be obtained at the 1% strain.

$$k = \frac{F}{\Delta L} \tag{5}$$

In the formula, the force  $F = (\sigma_1 - \sigma_3) \times A$ , the axial difference stress is calculated at a strain of 1%. The obtained axial differential stress  $(\sigma_1 - \sigma_3)$  is 78 kPa, and we can convert it to 0.78 kgf/cm². Based on specimen area equaling 39.59 cm², we can find F = 30.88 kg. Meantime,  $\Delta L = \varepsilon \times L = 0.01 \times 14.2$  cm = 0.14 cm. The spring coefficient k can be obtained by dividing the force F obtained above by the length change  $\Delta L$ . Using Equation (5), the spring coefficient (k) is calculated as 220 kgf/cm, the spring coefficient of the first cycle. Many papers [35–37] mentioned that G or E value decreases with increasing strain. However, few papers mentioned the relationship between k and strain. The model in this article requires the relationship between k value and strain; the strain increases due to the variation of k value as the cyclic number increases. We used the relationship between G and the cyclic number as the relationship between the spring coefficient k and the cyclic number.

After the first cycle's spring coefficient is calculated, the shear modulus (G) of the first five cycles of the specimen at A-2 is calculated, as shown in Table 2. The shear modulus (G) curve equation, which is  $G = 5884.9e^{-0.1t}$  kPa, is solved in Table 2 with the help of a command in Excel.

**Table 2.** Determine shear modulus using cyclic triaxial test in A-2.

		A-2			
Cyclic no.	1	2	3	4	5
shear modulus G (kPa)	5047.94	4163.75	3478.77	2977.94	2561.36

This study uses the shear modulus (G) curve equation of the first five cycles at point A as the basis for the spring coefficient (k) curve equation. The spring coefficient (k) of the first cycle is brought in from the above calculation  $k = 220 \, \text{kgf/cm}$ ; a spring coefficient (k) curve equation similar to the shear modulus (G) curve equation can be obtained, as shown in Figure 2. Since the number of liquefaction times of the sample at point A is 15, the number of cycles on the horizontal axis is changed to 15. Point A's spring coefficient can be obtained from this method as  $k = 244e^{-0.1t} \, \text{kgf/cm}$ . The spring coefficient is a variable that changes with time and will decrease as time increases. Table 2 uses the above spring coefficient equation to calculate the values for each of the 15 cycles.

Appl. Sci. 2024, 14, 4178 6 of 20

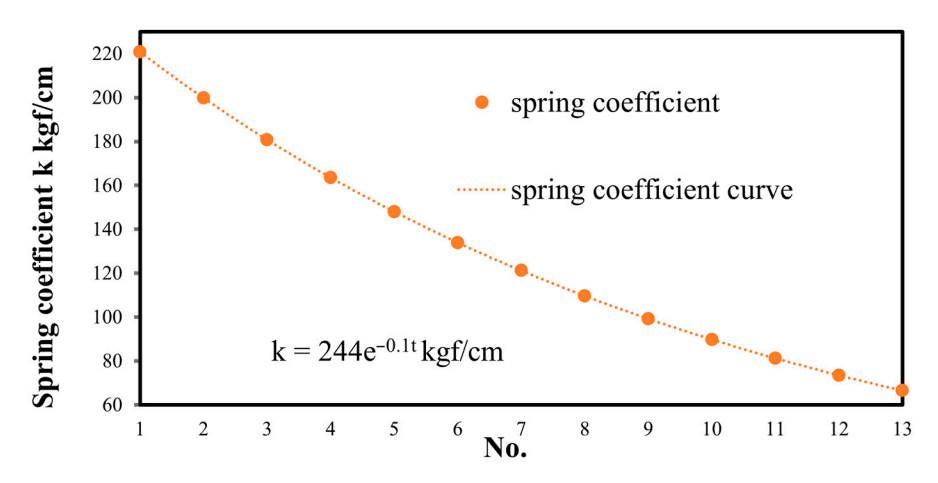


Figure 2. Spring coefficient versus cyclic no. in A-2 using cyclic triaxial test.

## Damping Coefficient

Kumar et al. and Akbarimehr and Fakharian [17,19] both mentioned the damping ratio (D) analysis method, such as Equation (6).

$$D = \frac{1}{4\pi} \frac{A_L}{A_T} \tag{6}$$

In which  $A_L$  is the area of the hysteresis loop, and  $A_T$  is the area of a shaded right triangle as Figure 3.  $A_L$  can be calculated by  $(\epsilon_1, \sigma_{d1})$ ,  $(\epsilon_2, \sigma_{d2})$ ,  $(\epsilon_3, \sigma_{d3})$  ...  $(\epsilon_n, \sigma_{dn})$  into Equation (7)

$$A_{L} = \frac{1}{2} \begin{vmatrix} \epsilon_{1} & \epsilon_{2} & \epsilon_{3} & \dots & \epsilon_{n} & \epsilon_{1} \\ \sigma_{d1} & \sigma_{d2} & \sigma_{d3} & \dots & \sigma_{dn} & \sigma_{d1} \end{vmatrix}$$
 (7)

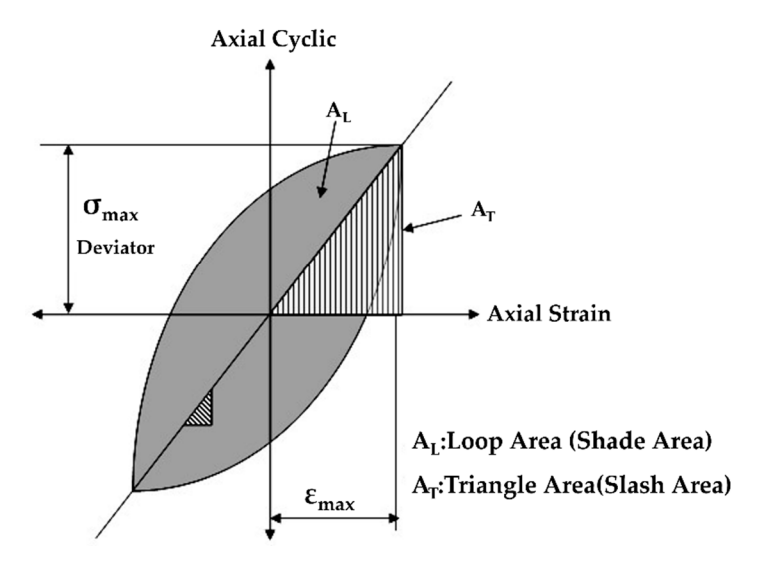


Figure 3. Stress-strain loop under load amplitude.

The damping coefficient c of site A is calculated in Figure 4. The damping ratio D obtained for each cycle of the cyclic triaxial test results of the specimen at site A is written in Table 3. Use the Excel trend line command to draw a set of equations directly used as the basis for the damping coefficient (c). Since the number of liquefaction times of the sample at point A is 15, the number of cycles on the horizontal axis is changed to 15, as shown in Figure 4. Point A's damping coefficient (c) can be obtained from the method as  $c = 0.739e^{-0.257t}$  kgf-s/cm. Table 3 uses the above damping coefficient equation to calculate the damping coefficients for 15 cycles.

Appl. Sci. 2024, 14, 4178 7 of 20

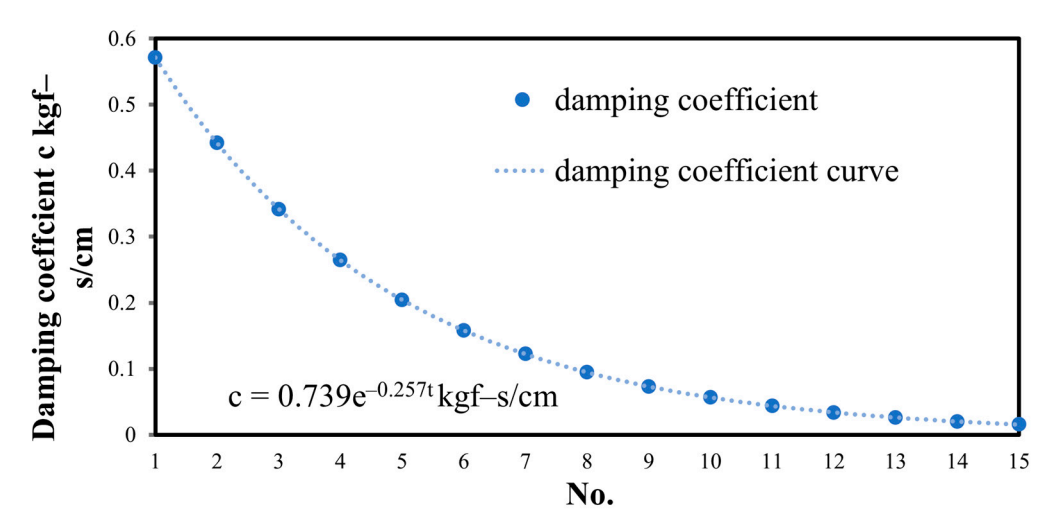


Figure 4. Damping coefficient versus cyclic no. in A-2 using cyclic triaxial test.

**Table 3.** Determine the damping ratio using the cyclic triaxial test in A-2.

		A-2			
Cyclic no.	1	2	3	4	5
damping ratio D	0.57	0.44	0.34	0.26	0.21

The external force  $(Q_0)$  calculation formula at point A is extended from Equation (8). The first cyclic spring coefficient (k) of point A can be obtained from  $k=220 \ kgf/cm$  stated before, multiplied by the strain of the first cycle of the specimen ( $\epsilon=0.323\%$ ), height (L = 14.2 cm), and  $\sin 2\pi t$ , as shown in Equation (8), the strain of the first cycle of the specimen is, and the external force in the liquefaction repeated triaxial test is a sinusoidal function cyclic loading. This study added  $\sin 2\pi t$  to the external force equation to simulate the cyclic triaxial test. Hence,  $Q_0$  is  $10.1\sin 2\pi t$  kg.

$$Q_0 = (k \times \varepsilon \times L) \times \sin 2\pi t \tag{8}$$

#### 2.3. Numerical Method to Solve It

After calculation by the above method and substituting each parameter into Equation (1), the formula of the sample from site A in the mass-spring-damping system can be obtained as Equation (9). Then, the specimen's strain will be solved by calculating it with Mathematica software.

$$1\ddot{z} + 0.739e^{-0.257t}\dot{z} + 244e^{-0.1t}z = 10.1\sin 2\pi t \tag{9}$$

First, enter the NDslove in the Mathematica command. The NDslove command is used to solve the numerical solution of a differential equation with variable coefficients. The result is a graph. The equation to be calculated, boundary conditions, and the range of variables need to be entered in the command. The equation to be calculated takes A-2 as an example, such as Equation (9). The boundary conditions in this study are set to 0 and 2. As for the range of time variable, because the cyclic number of liquefaction of the sample at point A approaches 15, we set the time to 15. After the graph of the NDslove results is solved, use the Plot command to draw the graph. In the Plot command, you also need to enter the range of the variables and the parameters to draw the graph. Since the number of liquefaction times of the sample at point A is 15, the range of the variables is the time (t) is set to 15. After the above two steps, the numerical solution of the quadratic differential equation with variable coefficients required in this study can be obtained.

To verify that the numerical solution obtained by the calculation software Mathematica is consistent with the analytical solution calculated using mathematical formulas, this

study first sets up a simple quadratic variable coefficient differential equation, such as Equation (10), by using Laplace transform and the calculation software Mathematica 12.1 to solve the problem, and by comparing the results, we can know the feasibility of Mathematica being used in the calculation of this study.

$$y'' + \frac{1}{3}e^{-0.2t}y' - \frac{51}{15}y = c(CSR)$$
 (10)

Substituting 0.2 for c in Equation (10), after calculating the analytical solution through Laplace transformation, use Excel to draw it and compare it with the numerical solution in Mathematica. Both times (t) are t=5 s. Substitute into the calculation, Figure 5 is a comparison chart of the Laplace transform and Mathematica results. It can be found that the two curves are consistent, so it can be verified that Mathematica is the calculation software that can be applied to this research.

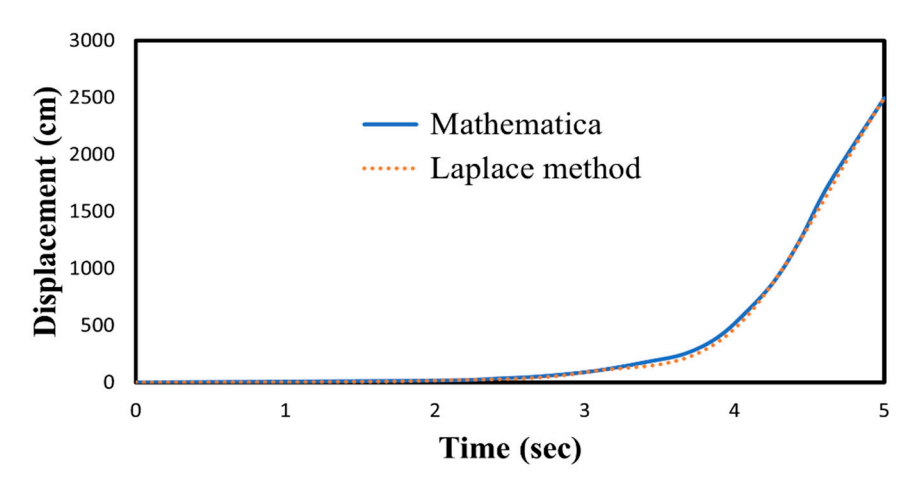


Figure 5. Numerical results comparison between the Laplace method and Mathematica.

## 3. Sensitivity Analysis of the Parameter

This part mainly discusses the parameters of the mass-spring-damping system, mass (m), spring coefficient (k), damping coefficient (c), and external force ( $Q_0$ ). The parameters used are based on point A. This is the result of the baseline calculation, which is reduced ten times and enlarged ten times one by one to discuss the impact on the simulated displacement of the mass-spring-damping system. The parameters discussed are in Table 4.

m-k-c System	Original	Reduced	Enlarged
Q <sub>0</sub> (kg)	$10.1\sin 2\pi t$	$1.01 \mathrm{sin} 2\pi \mathrm{t}$	101sin2πt
k (kgf/cm)	$244e^{-0.1t}$	$24.4e^{-0.1t}$	$2440e^{-0.1t}$
m (kg)	1	0.1	10
c (kgf-s/cm)	$0.739e^{-0.257t}$	$0.0739e^{-0.257t}$	$7.39e^{-0.257t}$

**Table 4.** Parameter range for every parameter.

## 3.1. Effect of Mass on Repeated Strain

In the beginning, the impact of changing the mass size (m) on the displacement of the mass-spring-damper system simulation is discussed. For this type, the mass (m) uses the calculation result m=1 kg as the original data. It reduces it by ten times and enlarges ten times; two different sizes of mass (m) can be obtained, m=0.1 kg and m=10 kg, respectively F1 to F3, as shown in Table 5, to explore the influence on simulated strain for the mass-spring-damping system.

Parameter in m-k-c		Value m		
No.	F1	F2	F3	
Q <sub>0</sub> (kg)	$10.1\mathrm{sin}2\pi\mathrm{t}$			
k (kgf/cm)	$244e^{-0.1t}$			
m (kg)	1	0.1	10	
c (kgf-s/cm)		$0.739e^{-0.257t}$		

**Table 5.** The parameter value for different mass m.

Bring the three sets of parameters obtained above into the mass-spring-damping system for calculation and explore the impact of reducing the mass (m) by ten times and enlarging it by ten times on the strain. After calculation with Mathematica software, the displacements from F1 to F3 can be obtained. The volume versus time graph is shown in Figure 6.

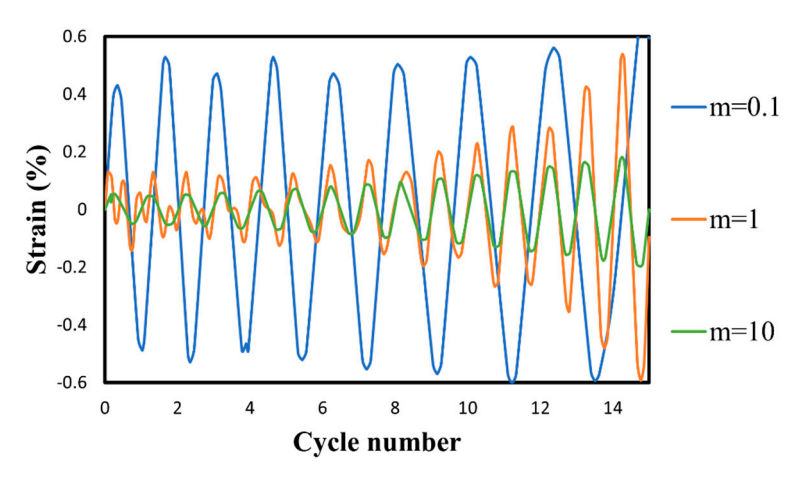


Figure 6. Strain versus cyclic number for different mass m.

It can be seen from Figure 6 above that based on the F1 original data  $m=1\ kg$ ; when the mass (m) is reduced ten times, the strain will be enlarged, and when the mass (m) is enlarged ten times, the displacement will be slightly reduced. Such a result can be imagined. When the size of the sample container is fixed, the relative density will increase as the mass increases. Thus, the strength will also increase, and the strain will decrease. This analysis result can be verified.

## 3.2. Effect of Spring Coefficient on Repeated Strain

Next, we will discuss the impact of changing the spring coefficient (k) on the simulated displacement of the mass-spring-damping system. For this type, the spring coefficient (k) is calculated based on the result  $k=244e^{-0.1t}\ kgf/cm$ . Original data, reduced ten times and enlarged ten times, two different sizes of spring coefficients (k) can be obtained,  $k=24.4e^{-0.1t}\ kgf/cm$  and  $k=2440e^{-0.1t}\ kgf/cm$ , respectively, G1 to G3, as shown in Table 6, to explore the impact on the simulated strain of the mass-spring-damping system.

**Table 6.** The parameter value for different spring coefficients, k.

Parameter in m-k-c		Value k	
No.	G1	G2	G3
Q <sub>0</sub> (kg)		10.1 sin2πt	
k (kgf/cm)	$244e^{-0.1t}$	$24.4e^{-0.1t}$	$2440e^{-0.1t}$
m (kg)		1	
c (kgf-s/cm)		$0.739e^{-0.257t}$	

Next, we will discuss the impact of changing the spring coefficient (k) on the simulated displacement of the mass-spring-damping system. For this type, the spring coefficient (k) is calculated based on the result  $k=244e^{-0.1t}\ kgf/cm$ . Original data, reduced ten times and enlarged ten times, two different sizes of spring coefficients (k) can be obtained,  $k=24.4e^{-0.1t}\ kgf/cm$  and  $k=2440e^{-0.1t}\ kgf/cm$ , respectively G1 to G3, as shown in Table 6, to explore the impact on the simulated strain of the mass-spring-damping system.

It can be seen from Figure 7 above that based on the original data of G1  $k = 244e^{-0.1t} \, kg/cm$ ; the displacement will be affected by the increase or decrease in the spring coefficient (k), which is an inverse but non-multiply relationship.

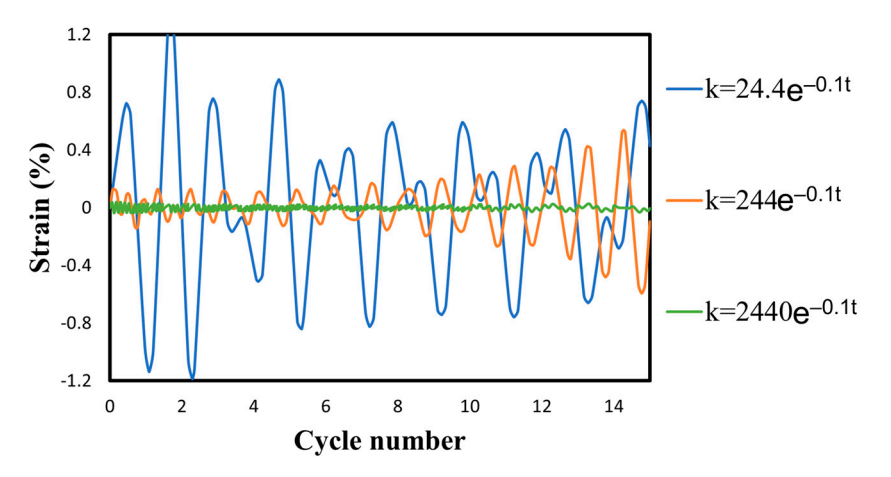


Figure 7. Strain versus cyclic number for different spring coefficient k.

### 3.3. Effect of Damping Coefficient on Repeated Strain

We continue to discuss the impact of changing the damping coefficient (c) on the simulated displacement of the mass-spring-damping system. For this type, the damping coefficient (c) is calculated, and the result is  $c = 0.739e^{-0.257t}$  kgf-s/cm is the original data, which is reduced by ten times and enlarged by ten times, respectively. Two damping coefficients (c) of different sizes can be obtained,  $c = 0.0739e^{-0.257t}$  kgf-s/cm and  $c = 7.39e^{-0.257t}$  kgf-s/cm, respectively, H1 to H3, as shown in Table 7, to investigate the influence on the simulated strain of the mass-spring-damping system.

Parameter in m-k-c		Value c		
No.	H1	H2	НЗ	
Q <sub>0</sub> (kg)		$10.1 \mathrm{sin} 2\pi \mathrm{t}$		
k (kgf/cm)		244e <sup>-0.1t</sup>		
m (kg)		1		
c (kgf-s/cm)	$0.739e^{-0.257t}$	$0.0739e^{-0.257t}$	$7.39e^{-0.257t}$	

**Table 7.** Parameter value for different damping coefficients c.

The above three sets of parameters were inserted into the mass-spring-damping system for calculation, and the impact of reducing and enlarging the damping coefficient c by ten times on the displacement was explored. After calculation with Mathematica software, the displacements from H1 to H3 can be obtained. The time graph is shown in Figure 8.

It can be seen from Figure 8 above that based on the H1 original data  $c = 0.739e^{-0.257t}$  kgf-s/cm, it can be found that the impact of the damping coefficient on the displacement could not be more precise.

Appl. Sci. 2024, 14, 4178 11 of 20

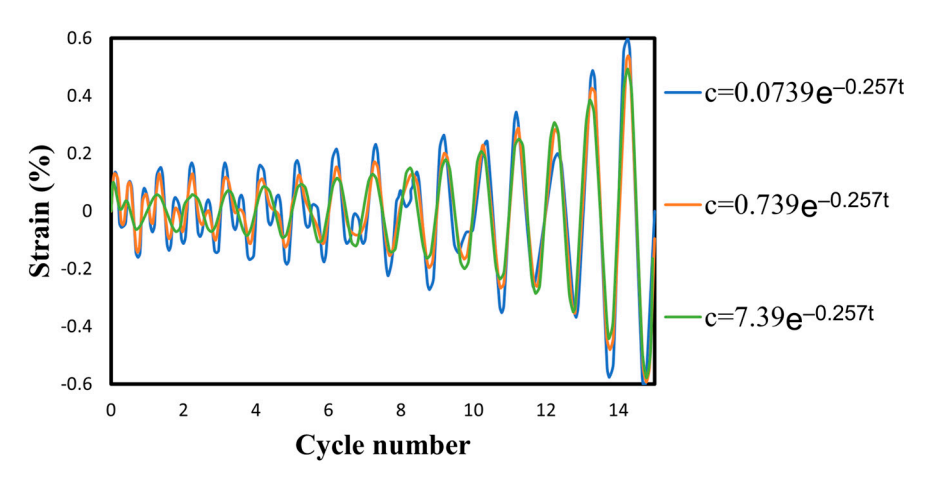


Figure 8. Strain versus cyclic number for different damping coefficient c.

## 3.4. Effect of External Force on Repeated Strain

Finally, the impact of changing the size of the external force  $(Q_0)$  on the simulated displacement of the mass-spring-damping system is discussed. For this type, the external force is reduced using the calculation result  $Q_0 = 10.1\sin 2\pi t$  kg as the original data. Ten times and ten times magnification, two different sizes of external forces  $Q_0$  can be obtained,  $Q_0 = 1.01\sin 2\pi t$  kg and  $Q_0 = 101\sin 2\pi t$  kg, respectively, I1 to I3, as shown in Table 8, to discuss the mass-spring-damping system when simulating the effect of the strain.

Parameter in m-k-c			
No.	I1	I2	I3
Q <sub>0</sub> (kg)	$10.1\sin 2\pi t$	$1.01 \mathrm{sin} 2\pi \mathrm{t}$	101sin2πt
k (kgf/cm)		$244e^{-0.1t}$	
m (kg)		1	
c (kgf-s/cm)		$0.739e^{-0.257t}$	

**Table 8.** The parameter value for different external force  $Q_0$ 

Substitute the above three sets of parameters into calculating the mass-spring-damping system to explore the impact of reducing the external force  $(Q_0)$  by ten times and amplifying it by ten times on the displacement. After calculation with Mathematica software, the displacements from I1 to I3 and the time chart are shown in Figure 9.

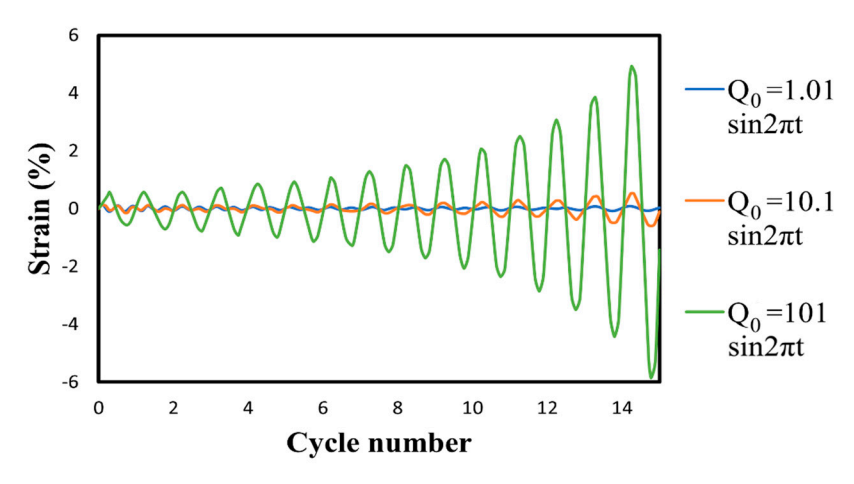


**Figure 9.** Strain versus cyclic number for different external force  $Q_0$ .

From Figure 9 stated above, we know that based on the original data of I1  $Q_0 = 10.1 \sin 2\pi t$  kg, the strain will be affected by the increase or decrease in the external force  $(Q_0)$ , and the two are proportional and seem not to be multiples.

From the preceding content, the summary of parameter analysis can be summarized as follows.

- 1. Mass (m) is a constant. According to the comparison result of changing the size of mass m, it can be found that it is inversely proportional to the displacement and is not a multiple. When the mass is reduced ten times, the displacement will be enlarged, and when the mass is reduced by ten times, the displacement will be enlarged. When the mass is enlarged ten times, the displacement will be slightly reduced.
- 2. The spring coefficient (k) is a variable that changes with time. According to the comparison results of changing the spring coefficient k, it can be found that the displacement will be affected by the increase or decrease in the spring coefficient in an inverse proportion and not a multiple relation.
- 3. The damping coefficient (c) is a variable that changes with time. According to the comparison results of changing the damping coefficient c, the impact of the damping coefficient on displacement could be more apparent.
- 4. The external force  $(Q_0)$  is the cyclic load multiplied by  $Sin2\pi t$ . According to the comparison results of changing the magnitude of the external force  $Q_0$ , it can be found that the displacement will be affected by the increase or decrease in the external force in a proportional and non-multiple relationship.
- 5. After reducing and enlarging the original data of spring coefficient k and damping coefficient c ten times and discussing, respectively, the influence of each parameter on the displacement can be obtained, as shown in Table 9.

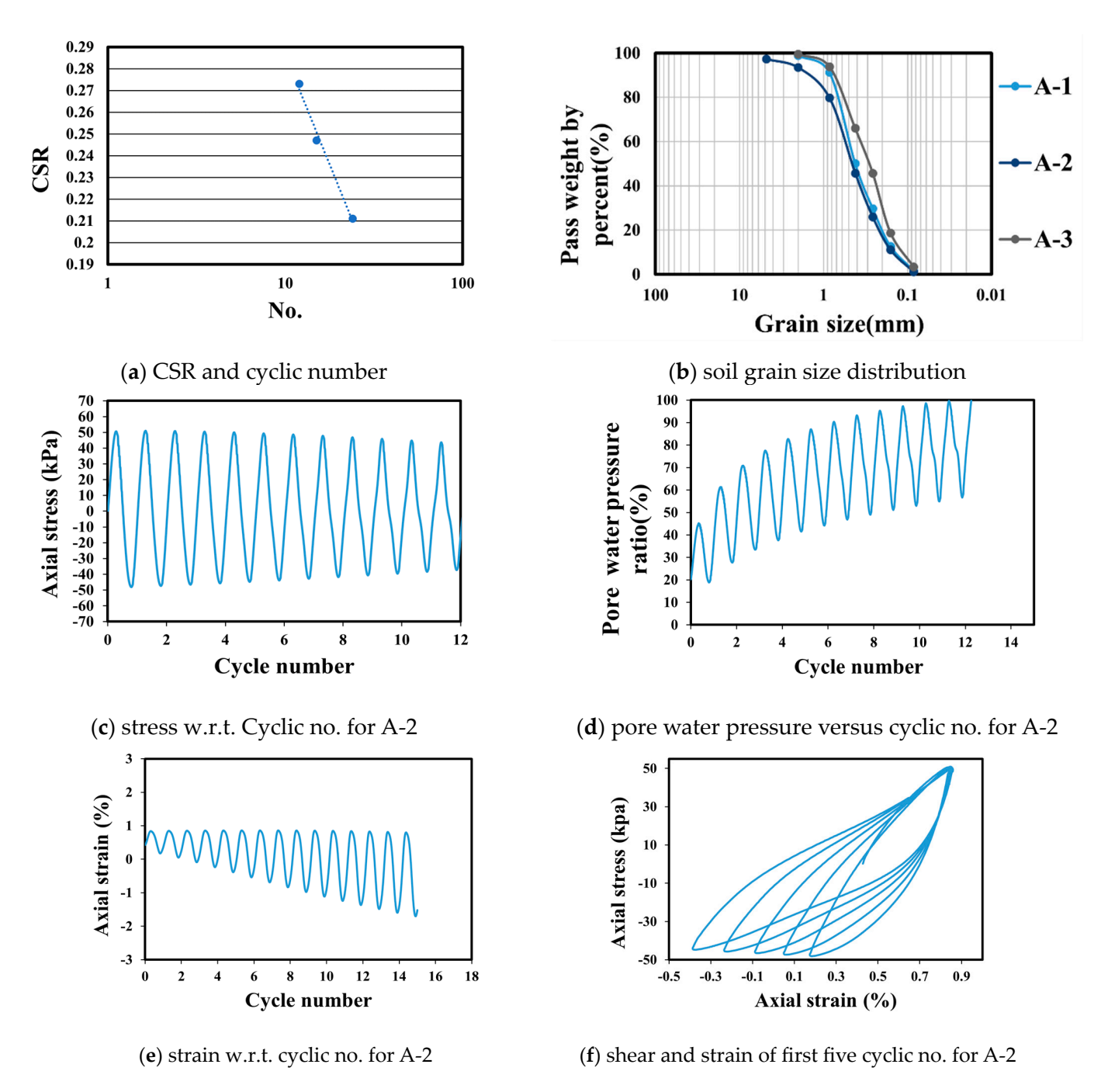
**Table 9.** Influence degree of each parameter of a mass-spring-damping system.

Parameter	Mass (m)	Spring Coefficient (k)	Damping Coefficient (c)	External Force $(Q_0)$
The degree of influence	medium	high	low	high

## 4. Results and Discussion

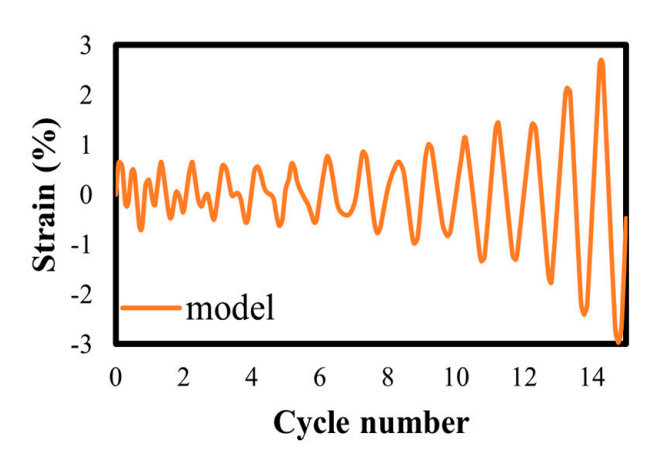
## 4.1. A Site

Point A is located in Huwei Town, Yunlin County, with a sampling depth of 5.0–5.75 m and a groundwater level of 2.3 m. The soil sample A-2 belongs to poorly graded sandy soil, and it is classified as SP according to the USCS method. The soil unit weight is 2.02 t/m<sup>3</sup>, the water content is 16.09%, and the specific gravity is 2.76. Figure 10a shows the soils liquefied at 15 cyclic times. Figure 10b indicates soil grain size distribution, from which most local soils are sandy soils, but the curve shows most soil particles contain a little fine. The shrinkage of the sample during cyclic loadings is not apparent for the A-2 specimen in Figure 10c, and we can find that the initial liquefaction occurred in the 10th cyclic number from the excess pore water ratio developed curve in Figure 10d. Figure 10e displays the double strain of the specimen with respective cyclic axial strain. Figure 10f is the stressstrain diagram of the first five cycles for A-2. Only the first five cycles are used because they are easier to analyze, and the analysis results are more accurate. The shear modulus of the first five cycles can be obtained, and click on each to get the shear modulus curve. The spring coefficient k of A-2 can be obtained as  $k = 244e^{-0.1t}$  kgf/cm. Due to liquefaction, the cyclic number of times is 15. The damping coefficient (c) of A-2 directly uses the damping ratio curve trend as the basis for the damping coefficient, and the damping ratio curve is obtained from the previous five cycles in Figure 10f. The damping coefficient c of A-2 can be  $c = 0.739e^{-0.257t}$  kgf-s/cm since the number of liquefaction times is 11.



**Figure 10.** The results of the cyclic liquefaction triaxial test for the sample at site A.

The mass m, damping coefficient c, spring coefficient k, and external force  $Q_0$  of point A are brought into the mass-spring-damping system calculation and compared with the liquefaction repeated triaxial test results, as shown in Figure 11. The strain of the first four cycles simulated by the mass-spring-damping system at point A has a relatively irregular amplitude, and the strain peak will have an upward trend as the number of cycles increases. The strain was obtained through repeated liquefaction triaxial tests. The peak value is flat, with no upward trend. After the eleventh cycle, there will be a more noticeable difference between the two. This may be related to the cumbersome simulation process and soil properties such as acceptable material content and ratio. The stress–strain diagram of this specimen is similar to taking the upper end of the block circle as the vertex and rotating clockwise from the lower left to the upper left; it is different from the stress–strain diagrams of the other three specimens.



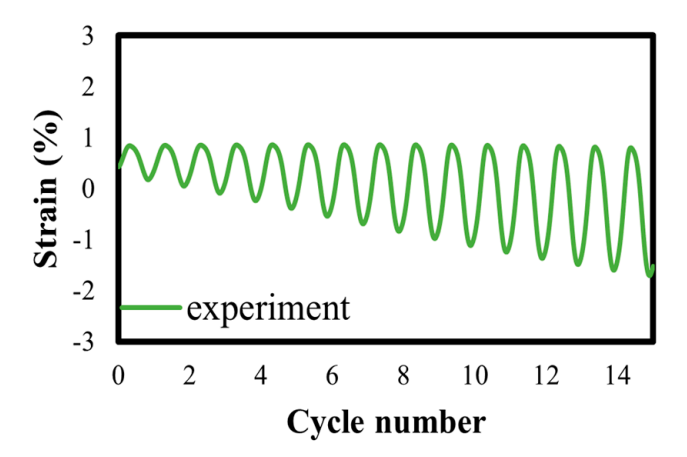


Figure 11. Comparison of strain and cyclic number between model and experiment for A-2.

4.2. B Site

Point B is located in Tuku Town, Yunlin County, with a sampling depth of 5.0-5.75 m and a groundwater level of 2.3 m. The soil sample B-2 is fine-graded silt-containing sand, SW-SM. The soil unit weight is  $2.02 \text{ t/m}^3$ , the moisture content is 22.44%, and the soil specific gravity is 2.69. We can obtain the cyclic number 18 when initial liquefaction is as in Figure 12a. Figure 12b shows soil grain size distribution, from which most local soils are sandy soils, but the data show all the soil particles passing 1 mm. The shrinkage is apparent and quick for the B-2 specimen in Figure 12c, although the initial liquefaction seems not to have occurred from the excess pore water ratio developed curve in Figure 12d. Figure 12e displays the double strain of the specimen with respective cyclic axial strain. The results are similar to those of Figure 10e. Figure 12f shows the stress–strain diagram of the first five cycles at point B. Only the first five cycles are used because they are easier to analyze, and the analysis results are more accurate. The result is the first cycle's spring coefficient k. The trend of the shear modulus G curve is the basis for the first cycle spring coefficient. The spring coefficient k of B-2 can be obtained as  $k = 269e^{-0.2t}$  kgf/cm because liquefaction times are 18 times. The damping ratio curve is obtained from the previous five cycles. The damping coefficient c of B-2 can be obtained as  $c = 0.298e^{-0.114t} \text{ kgf-s/cm}$ .

The mass m, damping coefficient c, spring coefficient k, and external force  $Q_0$  of point B are brought into the mass-spring-damping system calculation and compared with the results of the liquefaction repeated triaxial test, as shown in Figure 13. The strain peak value simulated by the mass-spring-damping system at point B increases as the number of cycles increases, but the strain peak value decreases at the eighth cycle. The strain peak value obtained through cyclic liquefaction triaxial tests rises more smoothly, and no shrinkage trend exists. There is a significant difference between the two in the first eight cycles. This may be related to the stress reduction and pore water pressure trend. The stress of the specimen reaches the fifth cycle. After that, it decreased significantly, and the pore water pressure ratio only rose to 50%, which did not reach the failure point of 100%.

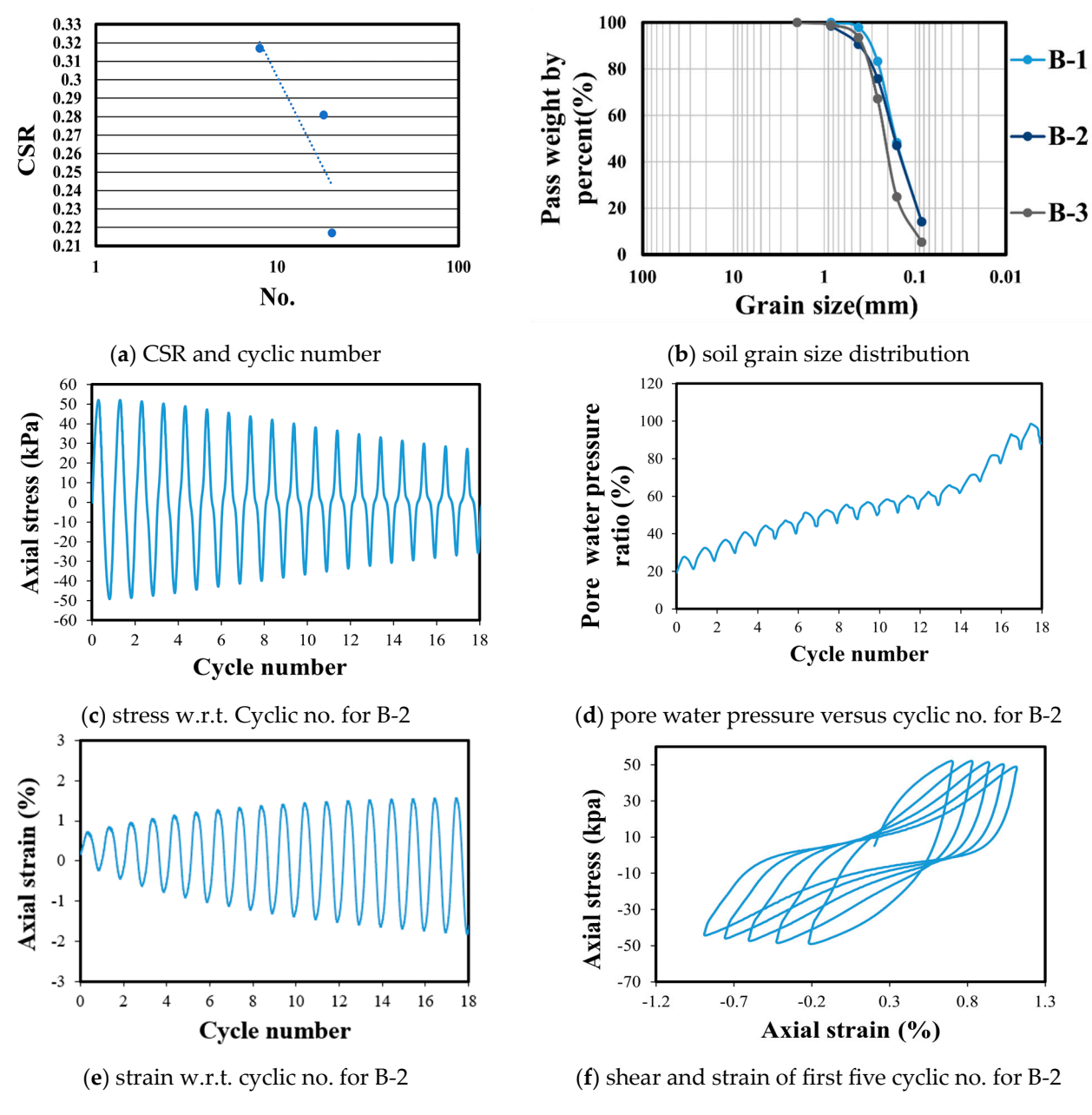


Figure 12. The results of the cyclic liquefaction triaxial test for the sample at site B.

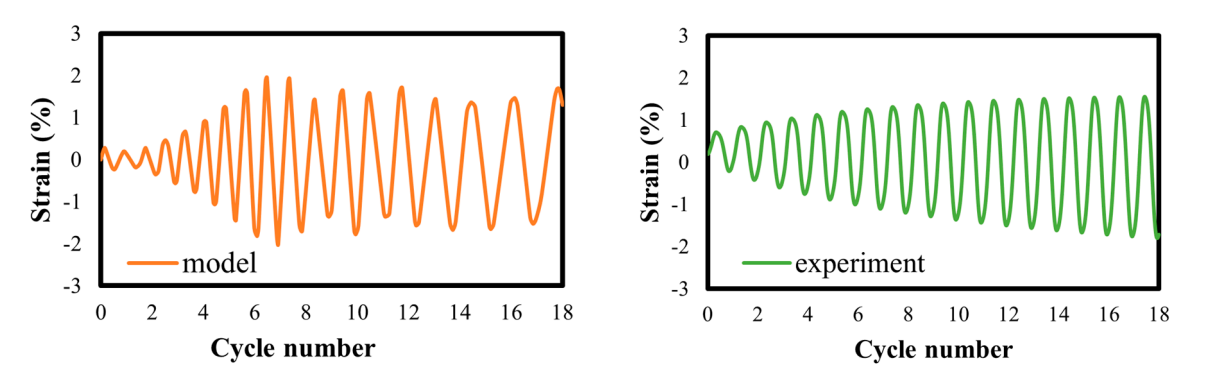
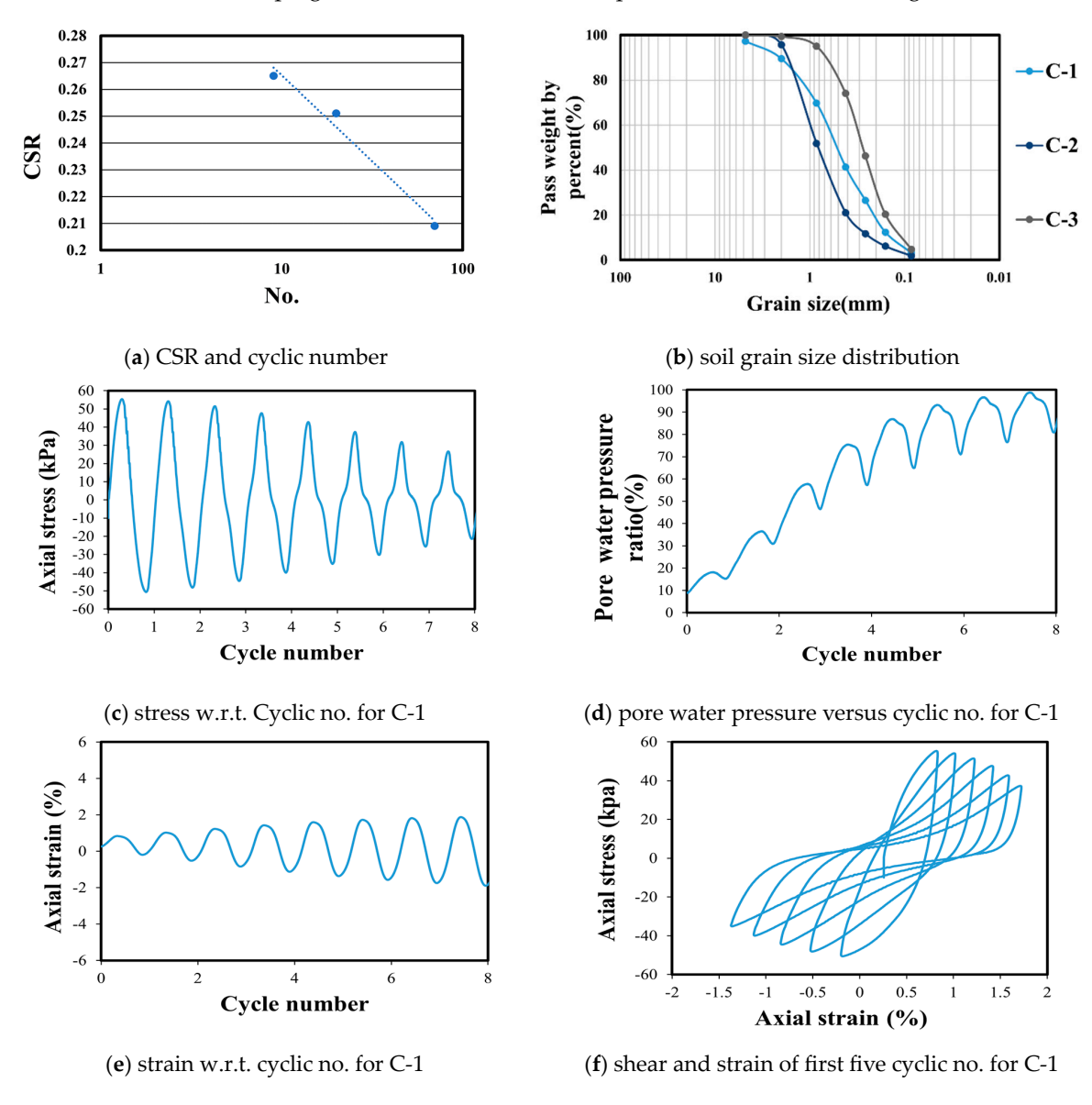


Figure 13. Comparison of strain and cyclic number between model and experiment for B-2.

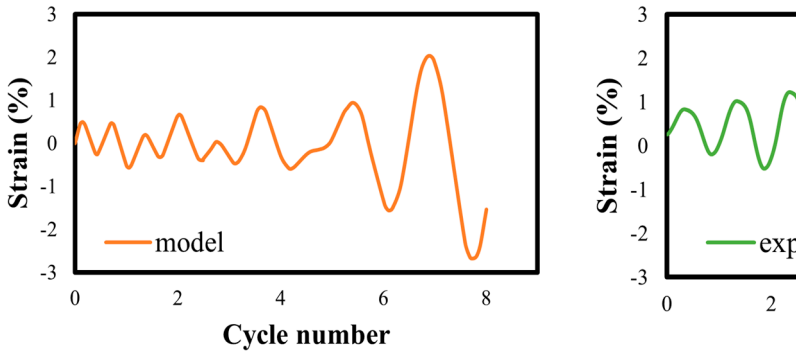
#### 4.3. C Site

Point C is located in Huwei Town, Yunlin County, with a sampling depth of 5.0 to 5.8 m and a groundwater level of 3.6 m. The soil sample C-1 is poorly graded sand, SP-SM. The soil unit weight is 2.12 t/m³, and the moisture content is 23.33%; soil specific gravity is 2.69. The sample C-1 was applied with an effective confined pressure of 100 kPa, and the cyclic stress ratio (CSR) is 0.265; then, we can obtain the cyclic number 9 when initial liquefaction in Figure 14a. Figure 14b shows soil grain size distribution, from which most local soils are sandy soils, but the fine content is very low. The shrinkage is apparent and quick for the C-1 specimen in Figure 14c, although the liquefaction cyclic number is seven from the excess pore water ratio in Figure 14d. However, Figure 14e displays that the double strain is from 2% to -2% during cyclic loadings and does not have considerable axial strain. Figure 14f below is the stress–strain diagram of point C for each cycle. Only the first five cycles are used because they are easier to analyze, and the analysis results are more accurate. The result is the first cycle's spring coefficient. The modulus curve trend is the basis for the first cycle spring coefficient. The spring coefficient k of C-1 can be obtained as  $k = 329e^{0.4t}$  kgf/cm. Since the number of liquefaction times is 9, the damping coefficient c of C-1 can be expressed as  $c = 0.356e^{-0.152t}$  kgf-s/cm.



**Figure 14.** The results of the cyclic liquefaction triaxial test for the sample at site C.

The mass m, damping coefficient c, spring coefficient k, and external force  $Q_0$  of point C are brought into the mass-spring-damping system calculation and compared with the results of the liquefaction repeated triaxial test, as shown in Figure 15. The strain peak value of the specimen at point C in the first six cycles simulated by the mass-spring-damping system is smaller than the results of the liquefaction repeated triaxial test. The strain peak value is reduced in the third and fifth cycles. The upward trend of the strain peak obtained from the axial test is relatively smooth, and there is no shrinkage trend. The difference between the two may be related to the cumbersome simulation process and the stress reduction of the specimen. The stress of the specimen began to decrease significantly after the second cycle.



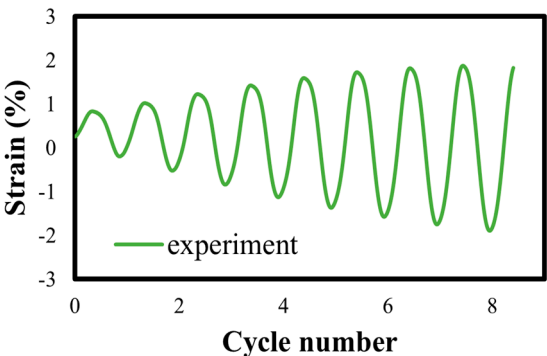


Figure 15. Comparison of strain and cyclic number between model and experiment for C-1.

## 4.4. D Site

Site D is located in Huwei Town, Yunlin County. The sampling depth is 11.0–11.75 m; the groundwater level is 5 m below ground level. The soil sample D-1 is silt (ML); the soil unit weight is 1.90 t/m<sup>3</sup>; the water content is 37.61%; and the specific gravity is 2.57. CSR and cyclic numbers are shown in Figure 16a. Figure 16b shows the distribution of soil grain size, which shows a high fine content for local soils. The liquefaction number is 13 for D-1 in Figure 16c, but the excess pore water pressure ratio almost reaches the initial liquefaction when the cyclic loading number comes near 12 in Figure 16d. However, Figure 16e displays that the double strain is from 3% to -1% during cyclic loadings and does not have considerable axial strain. Figure 16f shows the stress-strain diagram of the first five cycles at D-1. It can be found that there are two wrinkles in the blocking circle of these five cycles. The reason for the wrinkles may be that the silt in the thin tube is mixed with gravel. When two more complex particles are encountered, the stress decreases during the cyclic liquefaction triaxial test. Only the first five cycles are used because they are more accurate and easily analyzed. As stated above, the shear modulus of the first five cycles can be obtained. Based on the shear modulus curve trend as a basis for the first cycle spring coefficient), the spring coefficient k of D-1 can be obtained as  $k = 244e^{0.1t} \text{ kgf/cm}$  because the number of liquefaction times is 13 times. The damping coefficient c of D-1 directly uses the damping ratio curve trend as the basis for the damping coefficient, and the damping ratio curve is obtained from the previous five cycles. The damping coefficient c of D-1 can be obtained as  $c = 0.434e^{-0.07t} \text{ kgf-s/cm}$ .

All parameters were brought into the mass-spring-damping system calculation and compared with the liquefaction cyclic triaxial test results, as shown in Figure 17. The peak strain value simulated by the mass-spring-damping system at the D-1 sample will increase as the number of cycles increases. The peak strain value of the first six cycles is smaller than those of cyclic triaxial tests. The peak upward trend was smoother, but the overall trend was higher. It is symmetrical at 1% strain. It is different from the previous symmetry axis with 0%. If 0% is the symmetry axis, the upward direction of the strain curve is pressure, and the downward direction is extension. The reason is that the soil structure of the specimen may cause it, and the difference between the two in the first six cycles may be related to the

gradual reduction of the specimen's stress. The stress of the specimen began to decrease significantly in the third cycle.

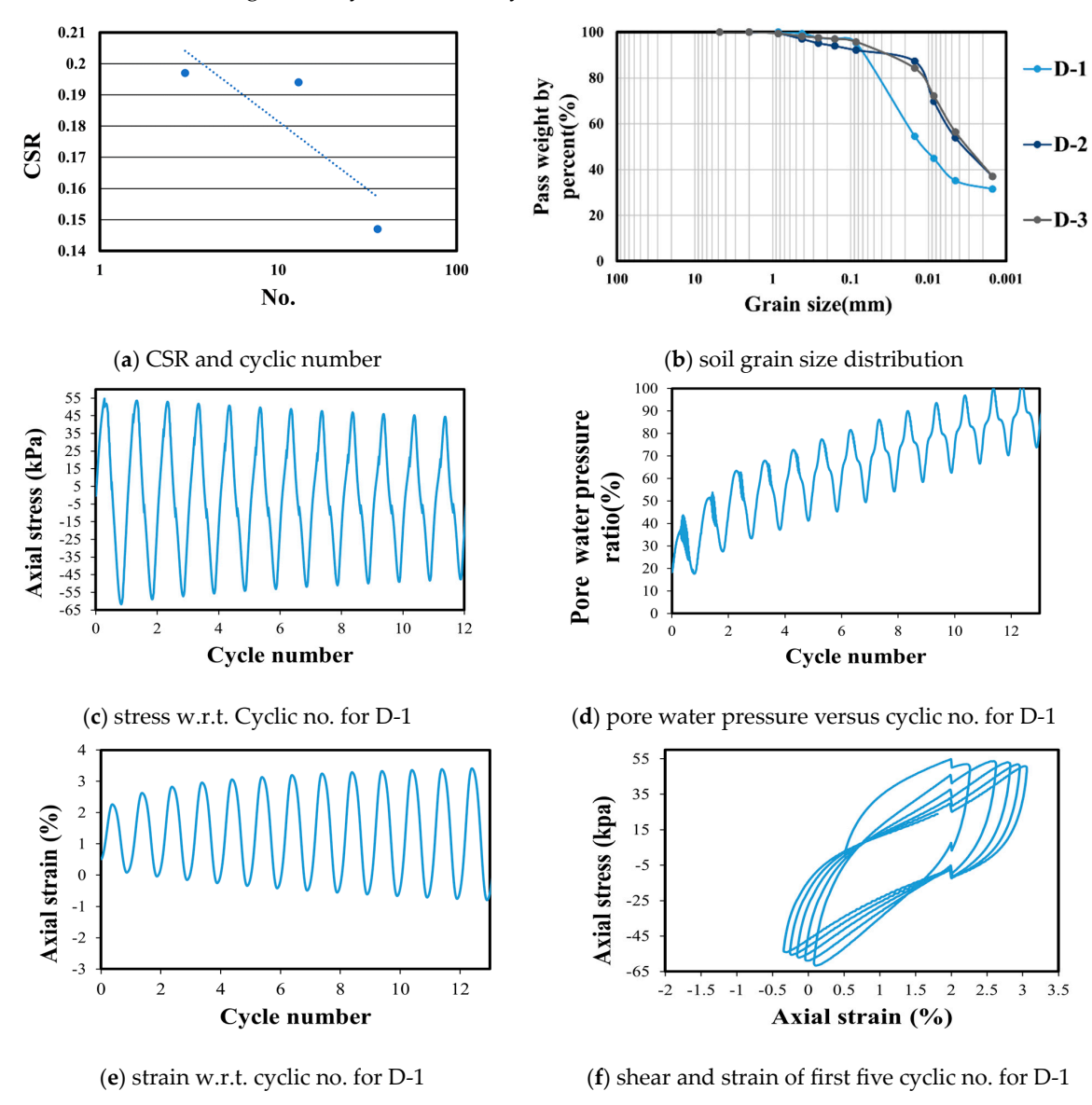


Figure 16. The results of the cyclic liquefaction triaxial test for the sample at site D.

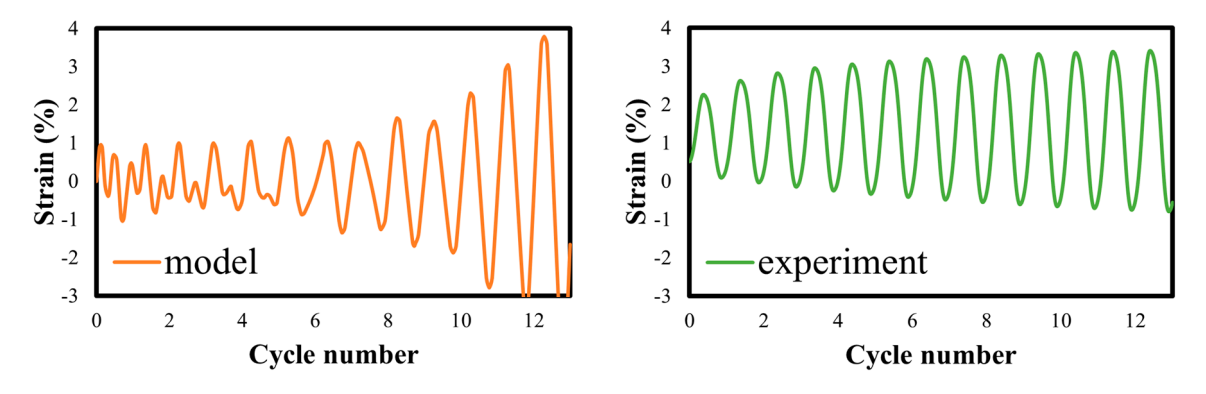


Figure 17. Comparison of strain and cyclic number between model and experiment for D-1.

#### 5. Conclusions

This study uses a mass-spring-damping system to simulate the repeated strain of liquefaction cyclic triaxial tests. For the sample at site A, Mathematica is used to solve the parameters required for the mass-spring-damping system, and each parameter in the mass system is discussed. Finally, the repeated strains simulated by the mass-spring-damping system are compared with those obtained by the liquefaction cyclic triaxial test. According to the relationship between the static triaxial test results and dynamic and static loads of past literature, the parameters of four points can be obtained. A Point is used as an example, and the mass of the sample at point A is m = 1 kg, the spring coefficient  $k=244e^{-0.1t}\ kgf/cm$ , the damping coefficient  $c=0.739e^{-0.257t}\ kgf-s/cm$ , and the external force  $Q_0=10.1sin2\pi t\ kg$ . This study discovered through the hysteresis loop of cyclic liquefaction triaxial tests that the spring and damping coefficients' parameters change with time.

By comparing the results of the mass-spring-damping system and liquefaction cyclic triaxial tests on soil samples from four different locations, preliminary results show that this model does not consider the increase in pore water pressure and the decrease in effective stress during repeated loading. Under this condition, the repeated strain amount obtained from cyclic triaxial tests can be simulated. The model is simple, and the parameters are easy to understand and obtain, which shows its extensibility. However, the equation to be solved is a variable coefficient equation, so numerical values must be used with software-assisted calculations. Generally, the first cycle number simulation will be less accurate because the pore water pressure of the specimen changes rapidly when the performance has just started. In contrast, the increase in subsequent cycles may be biased due to cyclic stress variation and soil plasticity during simulation. In the future, pure sand specimens created in the laboratory will be suggested for simulation.

**Author Contributions:** D.-H.H., project administration, experimental plan, supervision, writing—review, and editing; Y.-W.L., experimental work, analysis, validation, writing—original draft preparation; C.-S.H., supervision, writing. All authors have read and agreed to the published version of the manuscript.

Funding: This research received no external funding.

Institutional Review Board Statement: Not applicable.

Informed Consent Statement: Not applicable.

**Data Availability Statement:** The raw data supporting the conclusions of this article will be made available by the authors on request.

Conflicts of Interest: The authors declare no conflicts of interest.

## References

- 1. Tropeano, G.; Chiaradonna, A.; d'Onofriob, A.; Silvestri, F. A numerical model for non-linear coupled analysis of the seismic response of liquefiable soils. *Comput. Geotech.* **2019**, *105*, 211–227. [CrossRef]
- 2. Chiaradonna, A.; Tropeano, G.; d'Onofrio, A. Development of a simplified model for pore water pressure build-up induced by cyclic loading. *Bull. Earthq. Eng.* **2018**, *16*, 3627–3652. [CrossRef]
- 3. Finn, W.D.L.; Bhatia, S.K. *Prediction of Seismic Porewater Pressures*; International Society for Soil Mechanics and Geotechnical Engineering: London, UK, 1981; pp. 201–206.
- 4. Ivšić, T. A model for the presentation of seismic pore water pressures. Soil Dyn. Earthq. Eng. 2006, 26, 191–199. [CrossRef]
- 5. Park, T.; Park, D.; Ahn, J.K. Pore pressure model based on accumulated stress. Bull. Earthq. Eng. 2015, 13, 1913–1926. [CrossRef]
- 6. Chehab, A.G.; Naggar, M.H.E. Design of efficient base isolation for hammers and presses. *Soil Dyn. Earthq. Eng.* **2003**, 23, 127–141. [CrossRef]
- Novak, M. Foundations for shock-producing machines. Can. Geotech. J. 1983, 20, 141–158. [CrossRef]
- 8. Ulmer, K.J.; Green, R.A.; Rodriguez-Marek, A.; Mitchell, J.K. Energy-Based Liquefaction Triggering Model. *J. Geotech. Geoenvironmental Eng.* **2023**, 149, 04023105. [CrossRef]
- 9. Dafalias, Y.F.; Manzari, M.T. Simple plasticity sand model accounting for fabric change effects ASCE. *J. Eng. Mech.* **2004**, *130*, 622–634. [CrossRef]
- 10. Xu, L.Y.; Zhang, J.Z.; Cai, F.; Chen, W.Y.; Xue, Y.Y. Constitutive modeling the undrained behaviors of sands with non-plastic fines under monotonic and cyclic loading. *Soil Dyn. Earthq. Eng.* **2019**, *123*, 413–424. [CrossRef]

11. Di Benedetto, H.; Blanc, M.; Tiouajni, S.; Ezaoui, A. Elastoplastic model with loading memory surfaces (LMS) for monotonic and cyclic behaviour of geomaterials. *Int. J. Numer. Anal. Methods Geomech.* **2014**, *38*, 1477–1502. [CrossRef]

- 12. Matsui, M. A Constitutive model for cyclic viscoplasticity of soils. Soils Found. 1988, 28, 19–37. [CrossRef] [PubMed]
- 13. Kramer, S.L. Geotechnical Earthquake Engineering; Viacom Company: New York, NY, USA, 1996.
- 14. Seed, H.B.; Wong, R.T.; Idriss, I.M.; Tokimatsu, K. Moduli and damping factors for dynamic analysis of cohesionless soils. *J. Geotech. Eng.* 1986, 112, 1016–1032. [CrossRef]
- 15. Kaya, Z.; Erken, A.; Cilsalar, H. Characterization of elastic and shear moduli of Adapazari soils by dynamic triaxial tests and soil-structure interaction with site properties. *Soil Dyn. Earthq. Eng.* **2021**, *151*, 106966. [CrossRef]
- 16. Varghese, R.; Amuthan, M.S.; Boominathan, A.; Banerjee, S. Cyclic and postcyclic behavior of silts and silty sands from the Indo Gangetic Plain. *Soil Dyn. Earthq. Eng.* **2019**, 125, 105750. [CrossRef]
- 17. Kumar, S.S.; Krishna, A.M.; Dey, A. Evaluation of dynamic properties of sandy soil at high cyclic strains. *Soil Dyn. Earthq. Eng.* **2017**, *99*, 157–167. [CrossRef]
- 18. Qin, Y.; Xu, X.; Yan, C.B.; Wen, L.; Wang, Z.; Luo, Z.Q. Dynamic damping ratio of mudded intercalations with small and medium strain during cyclic dynamic loading. *Eng. Geol.* **2021**, *280*, 105952. [CrossRef]
- 19. Akbarimehr, D.; Fakharian, K. Dynamic shear modulus and damping ratio of clay mixed with waste rubber using cyclic triaxial apparatus. *Soil Dyn. Earthq. Eng.* **2021**, *140*, 106435. [CrossRef]
- 20. Pisanò, F.; Jeremić, B. Simulating stiffness degradation and damping in soils via a simple visco-elastic plastic model. *Soil Dyn. Earthq. Eng.* **2014**, *63*, 98–109. [CrossRef]
- 21. Chowdhury, I.; Tarafdar, R.; Ghosh, A.; Dasgupta, S.P. Dynamic soil structure interaction of bridge piers supported on well foundation. *Soil Dyn. Earthq. Eng.* **2017**, *97*, 251–265. [CrossRef]
- 22. Li, P.; Song, E.X. A viscous-spring transmitting boundary for cylindrical wave propagation in saturated poroelastic media. *Soil Dyn. Earthq. Eng.* **2014**, *65*, 269–283. [CrossRef]
- 23. Kim, U.; Kim, D.; Zhuang, L. Influence of fines content on the undrained cyclic shear strength of sand–clay mixtures. *Soil Dyn. Earthq. Eng.* **2016**, *83*, 124–134. [CrossRef]
- 24. Liu, Z.; Kim, J.; Hu, G.; Hu, W.; Ning, F. Geomechanical property evolution of hydrate-bearing sediments under dynamic loads: Nonlinear behaviors of modulus and damping ratio. *Eng. Geol.* **2021**, 295, 106427. [CrossRef]
- 25. Chattaraj, R.; Sengupta, A. Liquefaction potential and strain dependent dynamic properties of Kasai River sand. *Soil Dyn. Earthq. Eng.* **2016**, *90*, 467–475. [CrossRef]
- 26. Xu, L.Y.; Cai, F.; Chen, W.Y.; Zhang, J.Z.; Pan, D.D.; Wu, Q.; Chen, G.X. Undrained cyclic response of a dense saturated sand with various grain sizes and contents of nonplastic fines: Experimental analysis and constitutive modeling. *Soil Dyn. Earthq. Eng.* **2021**, 145, 106727. [CrossRef]
- 27. Hwang, J.H.; Yang, C.W.; Chen, C.H. Investigations on Soil Liquefaction during the Chi-Chi Earthquake. *Soils Found.* **2003**, *43*, 107–123. [CrossRef] [PubMed]
- 28. Chang, M.H.; Kuo, C.P.; Shau, S.H.; Hsu, R.E. Comparison of SPT-N-based analysis methods in evaluation of liquefaction potential during the 1999 Chi-Chi earthquake in Taiwan. *Comput. Geotech.* **2011**, *38*, 393–406. [CrossRef]
- 29. Fansuri, M.H.; Chang, M.H.; Saputra, P.D.; Purwanti, N.; Laksmi, A.A.; Harahap, S.; Puspitasari, S.D. Effects of various factors on behaviors of piles and foundation soils due to seismic shaking. *Solid Earth Sci.* **2022**, *7*, 252–267. [CrossRef]
- 30. Chiou, J.S.; Huang, T.J.; Chen, C.L.; Chen, C.H. Shaking table testing of two single piles of different stiffnesses subjected to liquefaction-induced lateral spreading. *Eng. Geol.* **2021**, *281*, 105956. [CrossRef]
- 31. Das, B.M. Principles of Soil Dynamics; PWS-KENT Publishing Company: Boston, MA, USA, 1993.
- 32. Kaya, Z.; Erken, A. Cyclic and post-cyclic monotonic behavior of Adapazari soils. *Soil Dyn. Earthq. Eng.* **2015**, 77, 83–96. [CrossRef]
- 33. Bray, J.D.; Markham, C.S.; Cubrinovski, M. Liquefaction assessments at shallow foundation building sites in the Central Business District of Christchurch, New Zealand. *Soil Dyn. Earthq. Eng.* **2017**, *92*, 153–164. [CrossRef]
- 34. Hsiao, D.H.; Phan, V.T.A.; Hsieh, Y.T.; Kuo, H.Y. Engineering behavior and correlated parameters from obtained results of sand–silt mixtures. *Soil Dyn. Earthq. Eng.* **2015**, 77, 137–151. [CrossRef]
- 35. Sitharam, T.G.; Govindaraju, L.; Srinivasa Murthy, B.R. Evaluation of liquefaction potential and dynamic properties of silty sand using cyclic triaxial testing. *Geotech. Test. J.* **2004**, *27*, 423–429. [CrossRef]
- 36. Sladen, J.A.; D'Hollander, R.D.; Krahn, J. The liquefaction of sands, a collapse surface approach. *Can. Geotech. J.* **1985**, 22, 564–578. [CrossRef]
- 37. Mondal, G.; Prashant, A.; Jain, S.K. Simplified seismic analysis of soil-well-pier system for bridges. *Soil Dyn. Earthq. Eng.* **2012**, 32, 42–55. [CrossRef]

**Disclaimer/Publisher's Note:** The statements, opinions and data contained in all publications are solely those of the individual author(s) and contributor(s) and not of MDPI and/or the editor(s). MDPI and/or the editor(s) disclaim responsibility for any injury to people or property resulting from any ideas, methods, instructions or products referred to in the content.